Chemical Science

View Online / Journal Homepage
Dynamic Article Links

Cite this: DOI: 10.1039/c1sc00475a

www.rsc.org/chemicalscience

EDGE ARTICLE

Dip-pen nanolithography of optically transparent cationic polymers to manipulate spatial organization of proteolipid membranes†

Yoshie Narui and Khalid S. Salaita*

Received 17th July 2011, Accepted 16th November 2011
DOI: 10.1039/c1sc00475a

Published on 01 December 2011 on http://pubs.rsc.org | doi:10.1039/C1SC00475A
Downloaded on 03 December 2011

Herein we report on an approach to use dip-pen nanolithography (DPN) to rapidly prototype nano- and microscale cationic polymer structures that guide the transport of lipid molecules in a fluid membrane. An atomic force microscope (AFM) tip is used to transfer poly(diallyldimethylammonium chloride) (PDAC) to a silica surface that templates the self-assembly of a phospholipid bilayer. Based on AFM and high-resolution optical microscopy data, DPN-generated PDAC structures are optically transparent and composed of up to three molecular layers of polyelectrolyte. We demonstrate that patterns can juxtapose mobile and immobile ligands in a supported lipid bilayer that simultaneously engages the epidermal growth factor receptor (EGFR) and adhesion receptors on the cell surface. In principle, DPN-generated polyelectrolyte structures have important applications in investigating supramolecular protein assemblies in living cells.

Introduction

The lateral movement of lipids and associated biomolecules within the cell membrane is one of the hallmarks of living cells.[1] These motions allow cells to dynamically respond to their surrounding environment, converting extracellular signals into internal chemical responses. Often, this can lead individual receptors to associate within the cell membrane forming hierarchical organizations that alter the kinetics and thermodynamics of their functions.[2–4] For example, specific receptors have been observed in microdomains separated by "picket-fences" or semi-permeable lipid diffusion barriers on the surface of many cells.[5,6] Nano- or microscale membrane corrals alter the higher order organization of receptor assemblies and subsequently influence the transmission of information across the cell membrane.[7,8] Given the importance of these protein assemblies, it is imperative that new methods are developed to investigate the role of protein and lipid compartmentalization in the surface of live cells.[5,9–15]

To address this need, nanopatterned supported lipid membranes have been introduced to direct the lateral diffusion of specific receptors in live cells.[16,17] Supported lipid bilayers are formed by the self-assembly of phospholipids onto an appropriate solid surface, such as silicon oxide or mica.[18,19] On these supporting materials, lipid molecules adopt a fully fluid membrane bilayer structure with molecular adlayers of water separating the substrate and lipid membrane.[19] This thin film of water is believed to help maintain the membrane structure and allow for lateral fluidity of the lipids. Ligands that are conjugated to the lipid headgroups are confined to the plane of the membrane and also display two-dimensional diffusion across the substrate. When nanoscale metal and metal oxide structures (100–500 nm lateral dimensions and 10 nm height) are fabricated onto the solid support using e-beam lithography, lipid molecules are unable to move across these nanostructures, and ligand mobility is restricted to specific pre-defined geometries.[7,9,20] Importantly, when cell surface receptors encounter their cognate ligands on the supported membrane, they too become subject to the constraints of the substrate diffusion barriers. The transport of ligand-receptor complexes and associated signaling molecules is only influenced through their interactions with the nano-patterned glass coverslip, which provides molecular specificity in cell manipulations.

While conventional metal nanostructures function as effective lipid diffusion barriers, they suffer from several challenges when used to investigate the role of receptor organization in cell signaling. The first relates to the relatively large extinction coefficient of metallic structures within the UV and visible range of wavelengths,[21] see Fig. S1 in the ESI.† This limits the utility of fluorescence microscopy as a characterization tool because a portion of the excitation and emission intensity will be selectively absorbed by the metal barriers. For example, in our hands, we find that 10 nm Cr nanopatterns reduce the measured fluorescence intensity of a 1 μM fluorescein solution by ~15% (Fig. S1 in the ESI†). Therefore, the optical properties of metallic nanostructures pose a challenge because imaging fluorescent

Department of Chemistry, Emory University, 1515 Dickey Drive, Atlanta, GA, 30322, USA. E-mail: k.salaita@emory.edu; Tel: +1-404-727-7522

† Electronic supplementary information (ESI) available: Information on fluorescence attenuation on e-beam patterned grids and representative images of the following: partially formed PDAC lines, NBD-PC bilayer on PDAC dot array, optical transparency of PDAC patterns, BSA-Cy3 localization on PDAC lines, PDAC dot array before the addition of cells and live cell interactions with PDAC lines. Table describing ink compositions and conditions tested and description of data analysis of EGFR activation levels. See DOI: 10.1039/c1sc00475a

Published on 01 December 2011 on http://pubs.rsc.org | doi:10.1039/C1SC00475A
Downloaded on 03 December 2011

proteins is a fundamental technique used in cell biology investigations. The second drawback relates to the serial nature of e-beam lithography.[22] Biological studies require statistically significant data sets, and, as such, high-throughput nanopatterning approaches are required to increase the utility of the nanopatterned supported membrane technique. The third potential disadvantage of metallic nanostructures pertains to their feature size, most importantly their height, which is typically 10 nm.[10] While the cell membrane may not be directly influenced by nanoscale topographical features, some theoretical and experimental data suggests that ligand-receptor sorting may be influenced by nanoscale topography.[23,24] Ideally, a biomimetic membrane should present minimal topographical features to the cell except for the desired proteins whose interactions with cell receptors are being investigated. Finally, thin-film deposited Cr structures cannot easily be chemically tailored, and it would be desirable to generate nanoscopic structures to control lipid diffusion that are amenable to chemical modification.[25]

DPN is a scanning probe-based lithographic technique that generates maskless patterns by directly transferring ink molecules from the tip of a scanning probe to the underlying substrate.[26,27] Recent advances in tip parallelization have led to high-throughput printing capabilities across centimeter length scales with sub-50 nm resolution, including the development of corollary techniques such as hard-tip soft spring lithography and polymer pen lithography techniques.[28,29] DPN is compatible with a wide range of ink and substrate combinations, and there are several examples demonstrating the deposition of polymer inks such as proteins,[30,31] dendrimers,[32] and polydimethylsiloxane (PDMS).[33]

The Mirkin group has further shown that DPN can be used for patterning conducting polymers, poly(aniline sulfonic acid) and polypyrrole, onto modified silicon surfaces for use in nanoscale electronic devices, demonstrating that electrostatic forces stabilize the charged polymer ink onto the surface.[34] In our study, we extend the functionality of poly(diallyldimethylammonium chloride) PDAC nanopatterns beyond the fields of molecular electronics and layer-by-layer assembly,[35] showing that these structures obstruct lipid diffusion and are mechanically robust enough to withstand cellular forces. Thus, they may be used to manipulate the spatial organization of ligand-receptor complexes.

Herein, we identify PDAC, Fig. 1A, as an optically transparent polymer that hinders the lateral diffusion of lipid molecules, adheres strongly to silicon oxide substrates, and is amenable for nanopatterning using the DPN technique. We find that DPN-generated PDAC structures guide the organization of laterally mobile and anchored cell surface receptors into specific geometries. Other groups have directly used atomic force microscopy-based lithography to selectively deposit or remove lipids in a range of applications.[12–15,36] However, to the best of our knowledge, this is the first report of direct writing and rapid prototyping of micro- and nanoscale structures for controlling lipid diffusion and for patterning protein ligands within a proteolipid membrane.

Results and discussion

Aside from metal or metal oxides, there are a limited number of materials that can prevent lipid membrane spreading and that are also compatible with nanoscale patterning approaches. Predicting molecular species that can function in this capacity is not straightforward; moreover, to the best of our knowledge, there are no reports of molecular nanostructures that can hinder the diffusion of lipid membranes. For example, the most commonly used inks in DPN or PDMS-based microcontact printing (μCP)[22] are functionalized alkane thiols that are known to support the formation of hybrid lipid monolayers.[37] To address this challenge, we empirically tested a range of molecular inks that were amenable to patterning on silica. This included silanes terminated with polyethylene glycol, alkanes and perfluorinated alkanes, and poly(ethyleneimine), but only PDAC was effective at impeding lipid diffusion. We suspect that PDAC confers these capabilities based on its propensity to adsorb multilayers of intact vesicles that do not support the formation of fluid bilayers.[38–41]

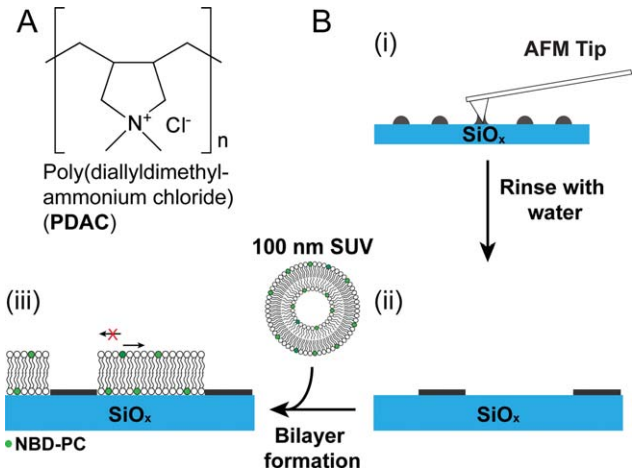

Fig. 1 (A) Chemical structure of PDAC polymer (n ~ 500). (B) Scheme of the DPN procedure: (i) deposition of PDAC on a silica substrate using an AFM tip, (ii) removal of excess polymer to form a thin film and (iii) formation of the supported lipid membrane. The lipids are laterally mobile except in the regions where the nanopatterned PDAC is located.

In a typical DPN experiment as depicted in Fig. 1B, etched glass coverslips were dried under a stream of N_2 and immediately used for DPN with an NScriptor system (see Experimental section). The PDAC polymer solution was applied to a one-dimensional, 24-tip F type pen array by immersing the tips into a small droplet of PDAC located on a nearby glass coverslip. The tips were subsequently blotted to remove excess ink, and then the tip array was brought into contact with the glass surface and levelled by observing changes in tip reflectivity.[27,29,42,43] In order to generate PDAC line structures, the tips contacted the surface and moved at a speed of 100 nm s^{-1} using an automated stage controller. After generating a set of lines, the stage was rotated by 90° where a second set of lines was deposited creating a grid pattern. The initial layer of polymer was tens of nanometers thick (data not shown), and the excess polymer layers were rinsed off with NanoPure water. The electrostatic interactions between the positively charged polymer and negatively charged glass surface were highly stable and allowed the patterns to remain robustly adhered under vigorous washes and across a range of ionic solution strengths.

To test the ability of the PDAC patterns to impede lipid diffusion, a lipid bilayer was allowed to form by incubating the

This journal is © The Royal Society of Chemistry 2011

Published on 01 December 2011 on http://pubs.rsc.org | doi:10.1039/C1SC00475A
Downloaded on 03 December 2011

patterned glass substrate with a solution of small unilamellar vesicles in phosphate-buffered saline (PBS) at pH 7.4, as shown schematically in Fig. 1B. In order to visualize lipid membrane diffusion with fluorescence microscopy, the lipid vesicles were doped with 2 mol% of fluorescent lipid, 1-oleoyl-2-{6-[(7-nitro-2-1,3-benzoxadiazol-4-yl)amino]hexanoyl}-*sn-glycero*-3-phosphocholine (NBD-PC). Fluorescence recovery after photobleaching (FRAP) experiments were performed on the grid, where a defined region of the lipid bilayer was photobleached and allowed to recover, see Fig. 2A. Fluorescence images of the as-fabricated structures before photobleaching (Fig. 2B) shows a series of 2 vertical and 3 horizontal polymer lines surrounded by a uniform lipid bilayer. The fluorescence image in Fig. 2C shows the same patterned lipid membrane region immediately after photobleaching. After 2.5 min, the lipid membrane underwent lateral diffusion such that the fluorescence intensity reached an equilibrium value within each corral, but intermixing across the polymer structures was hindered (Fig. 2D). The FRAP data demonstrates that DPN-generated PDAC line structures can inhibit lipid diffusion.

The formation of uniform PDAC lines was favored at low writing speeds, at or below 100 nm s^{-1}, and low polymer concentrations, 1 wt% PDAC. The polymer ink included 20% by vol ethylene glycol to reduce solvent evaporation and 58% by vol ethanol to assist transport of polymer from the tip to the glass surface. Note that in some cases, intermittent line patterns formed where incomplete polymer deposition occurred. Disjointed lines of PDAC were clearly observed with reflection interference contrast microscopy (RICM) (Fig. S2 in the ESI†). Importantly, such structures act as semi-permeable barriers that lower the effective diffusion rate but do not completely prevent lateral diffusion. Such structures mimic restricted diffusion in cells[6] and are desirable to study non-Brownian diffusion behavior of membrane bound molecules.[9]

In order to characterize the structure of PDAC adsorbates, dot arrays of the polymer were deposited onto an etched glass substrate and the remaining regions backfilled with a lipid membrane doped with NBD-PC (Fig. S3 in the ESI†). Such fluorescence images provided an indirect description of the size of the PDAC dot arrays. Using this analysis, we found that the optimum ink concentration for generating dot arrays consisted of a higher polymer concentration of 15.8 wt% PDAC (see Table 1 in the ESI†). In addition, we found that high spring constant tip arrays (1 N m^{-1}) with pre-fabricated ink channels were ideally suited for generating dot arrays. This is in agreement with the conditions that were recently employed to pattern PDMS dot arrays.[33] Using these conditions, a dot array was designed and fabricated in force-feedback mode under the InkCad software, where the dot-to-dot spacing was 2 μm and the total tip dwell time was 60 s. Given that the PDAC adsorbates are optically transparent, see Fig. S4 in the ESI,† dot arrays were immersed in a fluorescein solution to aid in rapid inspection and identification of the regions for AFM imaging (Fig. 3A). The fluorescent PDAC dot array was imaged in AC mode with a clean, premounted AC probe tip in order to avoid deforming the deposited structures. The phase image (Fig. 3C) indicated that the average dot diameter was 300 nm, but the topographical scan (Fig. 3D) showed no detectable features. To verify this observation, two line scans are plotted over identical regions across the center of a single dot in the phase and height AFM channels in Fig. 3B. Phase imaging has often been used for mapping differences in chemical composition, adhesion or viscoelasticity.[44] This result implies that the PDAC layers are chemically distinct, but their thickness cannot be distinguished from the root-mean-square roughness of the glass surface (~8 Å). Previous AFM studies of PDAC multilayer films agree with these findings and indicate that PDAC layers deposited at low ionic strength (<0.1 M NaCl) tend to adopt an extended rod-like conformation.[45,46] The thickness of polyelectrolyte

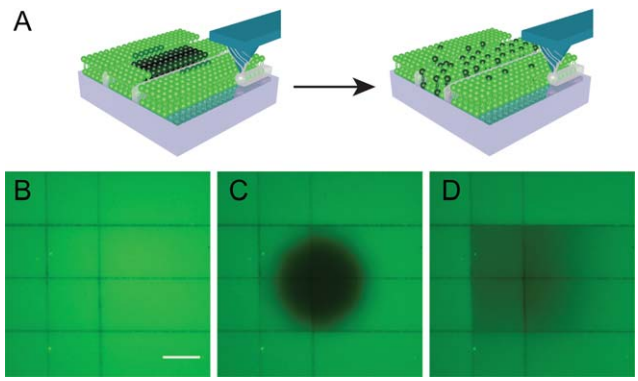

Fig. 2 (A) Schematic illustration of the FRAP experiment. (B) Representative fluorescence microscopy image of a supported lipid membrane doped with NBD-PC, and patterned with PDAC line structures deposited by DPN. Fluorescence images of the same region immediately after photobleaching (C), and 2.5 min after photobleaching (D). Scale bar = 25 μm.

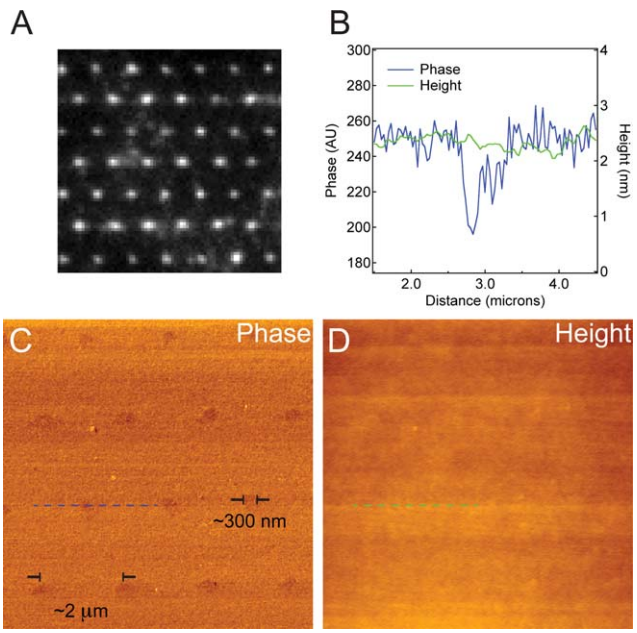

Fig. 3 (A) Representative fluorescence image of fluorescein-doped PDAC dot array generated on a glass substrate (Fig. 1Bii). The image is 12 μm × 12 μm. (B) Plots of AC mode AFM height and AFM phase of line scans taken from a single 300 nm dot from the array shown in (A). (C) AFM phase image, and (D) AFM height image of the PDAC dot array in (A). The dashed lines indicate the location of the regions that were plotted in (B). AFM images were collected with a scan size of 7.5 μm × 7.5 μm and scan rate of 1.0 Hz.

Published on 01 December 2011 on http://pubs.rsc.org | doi:10.1039/C1SC00475A
Downloaded on 03 December 2011

multilayer films (10 bilayers) range from 6–9 nm, thus indicating that the thickness of a single layer of polyelectrolyte ranges from 3–4.5 Å.[45,47] Taken together, this data indicates that DPN-deposited films consist of 1–3 molecular layers of PDAC and are responsible for hindering lipid mobility.

One of the major challenges in the area of supported membranes pertains to the ability to juxtapose mobile proteins and lipid alongside immobile proteins. The PDAC patterns created by DPN address this issue, as they provide a template for protein adsorption, while the phospholipid membrane prevents non-specific adsorption of biomolecules. To target protein binding to the PDAC lines, the nanopatterned supported membrane was exposed to a solution of 100 μg mL^{-1} bovine serum albumin (BSA) fluorescently tagged with Cy3 (BSA-Cy3). The BSA-Cy3 localized to the polymer lines and was not observed to adhere to the supported lipid membrane, as seen in Fig. S5 in the ESI.†

To demonstrate that the PDAC molecular layers can engage and manipulate the organization of cell surface receptors, we generated nanopatterned lipid membranes and coupled these to live cells. In particular, we sought to spatially immobilize integrin adhesions to the nanopatterned regions while allowing the molecular assembly of a free-floating cell receptor, such as the epidermal growth factor receptor (EGFR), within the fluid membrane surface. This was important because EGF-EGFR complexes are known to dynamically form higher-order oligomers at the cell surface.[48–52] Fibronectin conjugated to Cy3 fluorescent dye (FN-Cy3) was immobilized onto the PDAC regions, while the epidermal growth factor (EGF-Alexa Fluor 647) ligand was tethered to the upper leaflet of a supported lipid membrane as shown in Fig. 4A.

The breast cancer cell line, HCC1143, was selected for this experiment because it is an adherent cell line known to overexpress EGFR. Initially, the dot array was patterned and rinsed, followed by vesicle fusion to form the biotin functionalized membrane bilayer. The surface was incubated with 50 μg mL^{-1} FN-Cy3 for 30 min and then blocked with 100 μg mL^{-1} BSA to minimize any non-specific adsorption to the PDAC pattern. Streptavidin at 1 μg mL^{-1} and EGF-647 at 1 μg mL^{-1} were added sequentially to the bilayer to complete the surface preparation. Finally, RPMI media with 10% fetal bovine serum was exchanged into the sample chamber and 600,000 cells, in two aliquots, were incubated on the surface for 30 min at 37 °C and 5% CO_2. After 30 min of live cell imaging, the samples were fixed and stained for activation of EGFR through phosphorylation of the tyrosine residue at position 1068 (pY-1068).

A representative set of brightfield and fluorescence microscopy images show three cells adhered to a nanoscale dot array (Fig. 4B). RICM, which provides a measure of the distance between a cell membrane and the underlying support,[53] shows that the cells were tightly adhered to the dots presenting fibronectin. Note that the dot array maintained strong attachment to the glass slide despite cell adhesion and the application of tension across dots. Additional experiments indicated that polymer lines were able to withstand interactions with the cell (Fig. S6 in the ESI†). Fluorescence imaging of EGF-647 reveals the formation of EGF-EGFR clusters that translocate to the center of the cell-surface junction, presumably though a retrograde flow mechanism.[51] Importantly, some of the EGF clusters remain constrained by the immobilized fibronectin dots, indicating that these PDAC-FN-Cy3 adsorbates serve to restrict the motions of

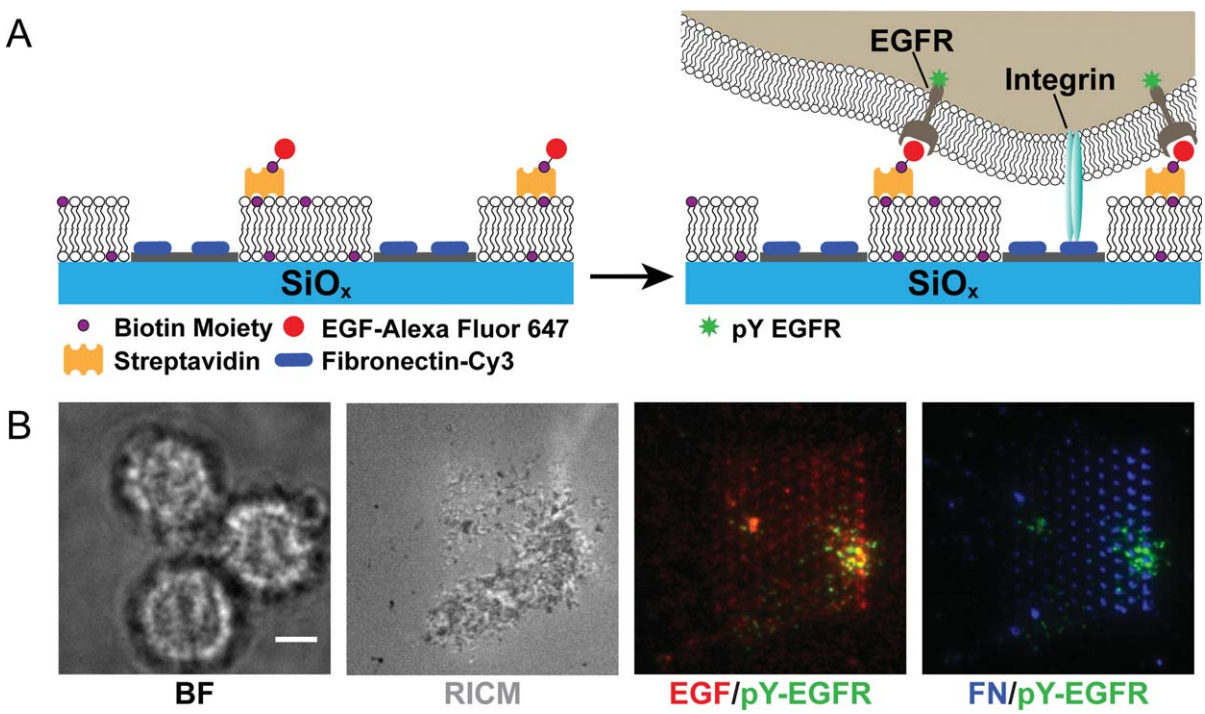

Fig. 4 (A) Scheme illustrating the binary ligand system that presents immobilized FN-Cy3 and laterally mobile EGF-647. The EGF and fibronectin ligands bind EGFR and integrins, respectively, when the substrate is interfaced with a live cell. (B) Representative brightfield, RICM, and fluorescence microscopy images of three cells that are engaged to a nanopatterned supported membrane. The overlaid images are false colored to aid in visualizing EGF/pY-EGFR and FN/pY-EGFR. Scale bar = 5 μm.

 This journal is © The Royal Society of Chemistry 2011

Published on 01 December 2011 on http://pubs.rsc.org | doi:10.1039/C1SC00475A
Downloaded on 03 December 2011

the EGFR in the cell membrane. There is a small amount of non-specific binding of EGF-647 onto the PDAC, implying that BSA blocking was not complete, though it is possible that other compounds such as PEG or casein may be more effective at preventing undesired protein binding to the polyelectrolyte. In spite of this, the pY antibody stain revealed that ~84% of the total pY signal, representing activated EGFR, is found in the fluid regions of the membrane and not over the immobilized fibronectin (see ESI for a description of data analysis†), thus suggesting that the non-specifically bound EGF-647 is notably less biologically active in comparison to the membrane-bound EGF species.

Conclusions

We have developed a new method for controlling ligand spatial organization in synthetic membranes and cells by using DPN to pattern PDAC, an optically transparent polyelectrolyte. We have shown that PDAC effectively impedes lipid diffusion, although its precise mechanism of lipid membrane interaction remains unclear. Based upon our AFM measurements, we rule out the possibility that the polymer acts as a topographical barrier, since the film thickness is below ~8 Å. This system can be used to understand the role of altered receptor spatial organization, such as that found in neuronal and immunological synapses as well as force transduction in adhesion contacts when coupled with recently developed force sensing methods at membranes.[54] Using this platform, one protein of interest was immobilized onto the PDAC pattern while a second protein was tethered to the laterally mobile lipid surface, recapitulating a biological membrane and avoiding the introduction of distinct topographical features. Our preliminary data with laterally mobile EGF and immobilized fibronectin is one of hundreds of possible ligand pairs that can be investigated using this approach. The technique offers significant advantages in terms of throughput, simplicity, and biological relevance compared to many previous approaches for receptor manipulations and especially given the recent development of massively parallel DPN-based patterning capabilities.

Experimental section

Materials

PDAC (M_w = 100,000 g mol^{-1}), 35 wt% in water, paraformaldehyde and Triton X-100 were purchased from Sigma Aldrich, USA. Ethanol, ethylene glycol, 25 mm diameter #2 glass coverslips and BSA were acquired from VWR, USA. F- and M-type pen arrays and premounted AC mode tips were purchased from NanoInk, Inc., USA. All lipids were obtained from Avanti Polar Lipids, USA. Human fibronectin was purchased from Innovative Research, USA and labeled with reactive Cy3 dye from GE Healthcare Life Sciences, USA. Recombinant human EGF was purchased from R&D Systems, USA. Alexa Fluor 647 carboxylic acid, succinimidyl ester and the secondary goat anti-rabbit IgG antibody conjugated with Alexa Fluor 488 were from Invitrogen, USA. Streptavidin was acquired from Rockland Immunochemicals, Inc., USA. Primary rabbit monoclonal antibody for pY (D7A5) was purchased from Cell Signaling Technology, USA.

DPN and AFM experiments

All DPN and AFM experiments were performed using the NScriptor DPNWriter nanolithography platform from NanoInk, Inc., USA, and the dot arrays were patterned using the InkCad software. The ink solution typically used to generate grid arrays consisted of a mixture of 1 wt% PDAC, 21% water, 58% ethanol, and 20% ethylene glycol by vol. The following ink solution mixture was typically prepared to generate dot arrays: 15.8 wt% PDAC, 29.2% water, 10% ethanol, and 45% ethylene glycol by vol. In order to load the tip with ink, the AFM cantilever was brought into contact with a 0.5 μL drop of the appropriate ink solution that was pipetted onto a clean glass slide. All glass substrates for DPN were piranha etched (H_2O_2: H_2SO_4; 1 : 3; v:v) for 15 min and rinsed 3 times with copious amounts of NanoPure water (Caution: piranha solution is an extremely strong oxidant and can become explosive if mixed with organics). DPN was carried out under ambient conditions of 22–25 °C and 25–40% relative humidity. AFM images were recorded in AC mode with the NScriptor.

Bilayer formation

After PDAC pattern fabrication, samples were rinsed with copious amount of NanoPure water. Substrates were then incubated with a 30 μL solution consisting of 15 μL of PBS and 15 μL of a 2 mg mL^{-1} solution of lipid vesicles. For FRAP experiments, the lipid vesicle solution was composed of 98 mol% 1,2-dioleoyl-*sn*-*glycero*-3-phosphocholine (DOPC) and 2 mol% NBD-PC. For cell experiments, the solution was comprised of 99.9 mol% DOPC and 0.1 mol% 1,2-dioleoyl-*sn*-*glycero*-3-phosphoethanolamine-*N*-(cap biotinyl) (biotin-PE). The vesicles were prepared according to previously published methods.[52] Note that each incubation step was followed by rinsing with 50 mL of 1 × PBS.

Fluorescence imaging

All fluorescence images were collected on a Nikon Ti Eclipse microscope featuring an Evolve EM CCD (Photometrics), an Intensilight epifluorescence source (Nikon), and a total internal reflection fluorescence (TIRF) launcher with two laser lines: 488 nm (10 mW) and 647 nm (20 mW). The microscope also includes the Nikon Perfect Focus System, an interferometry-based focus lock. The microscope is equipped with Chroma filter cubes, of which the following were used for experiments in this paper: TIRF 488, TIRF 647, Cy5, TRITC, FITC, and RICM. Images were collected using Nikon's NIS Elements software and analyzed using ImageJ software from NIH. For FRAP experiments, the samples were illuminated in an epifluorescence configuration while the cells were imaged in TIRF mode to minimize autofluorescence and image the interface between the cell membrane and the supported lipid membrane. The exception to this was the FN-Cy3, which was imaged in epifluorescence.

Cell experiments

Cells were fixed by rinsing with cold PBS to remove media and treated with a 4% paraformaldehyde solution for 12 min. After rinsing with 1 × PBS, the cells were permeated with 0.1% Triton

X-100 for 5 min, rinsed, and stored overnight in a 1% BSA in 1 × PBS solution. The primary antibody was diluted 1 : 200 in 1% BSA and incubated for 1 h. The sample was thoroughly rinsed and incubated with the secondary antibody at a dilution of 1 : 1000 for 30 min. After a final rinse, the fixed cells were ready for imaging.

Acknowledgements

This project was supported by ORNL user proposal CNMS2009-269, Emory Winship Cancer Institute and the Georgia Cancer Coalition Cancer Research Award. The authors would like to thank Daniel Stabley for his help creating the table of contents figure.

Notes and references

1 S. J. Singer and G. L. Nicolson, *Science*, 1972, **175**, 720.
2 J. Gureasko, W. J. Galush, S. Boykevisch, H. Sondermann, D. Bar-Sagi, J. T. Groves and J. Kuriyan, *Nat. Struct. Mol. Biol.*, 2008, **15**, 452.
3 D. Holowka, J. A. Gosse, A. T. Hammond, X. Han, P. Sengupta, N. L. Smith, A. Wagenknecht-Wiesner, M. Wu, R. M. Young and B. Baird, *Biochim. Biophys. Acta, Mol. Cell Res.*, 2005, **1746**, 252.
4 S. Bromley, W. Burack, K. Johnson, K. Somersalo, T. Sims, C. Sumen, M. Davis, A. Shaw, P. Allen and M. Dustin, *Annu. Rev. Immunol.*, 2001, **19**, 375.
5 M. Wu, D. Holowka, H. G. Craighead and B. Baird, *Proc. Natl. Acad. Sci. U. S. A.*, 2004, **101**, 13798.
6 N. L. Andrews, K. A. Lidke, J. R. Pfeiffer, A. R. Burns, B. S. Wilson, J. M. Oliver and D. S. Lidke, *Nature*, 2008, **10**, 955.
7 K. D. Mossman, G. Campi, J. T. Groves and M. L. Dustin, *Science*, 2005, **310**, 1191.
8 B. N. Manz and J. T. Groves, *Nat. Rev. Mol. Cell Biol.*, 2010, **11**, 342.
9 J. Tsai, E. Sun, Y. Gao, J. C. Hone and L. C. Kam, *Nano Lett.*, 2008, **8**, 425.
10 K. Salaita, P. M. Nair, R. S. Petit, R. M. Neve, D. Das, J. W. Gray and J. T. Groves, *Science*, 2010, **327**, 1380.
11 P. M. Nair, K. Salaita, R. S. Petit and J. T. Groves, *Nat. Protoc.*, 2011, **6**, 523.
12 J. Shi, J. Chen and P. S. Cremer, *J. Am. Chem. Soc.*, 2008, **130**, 2718.
13 S. Lenhert, F. Brinkmann, T. Laue, S. Walheim, C. Vannahme, S. Klinkhammer, M. Xu, S. Sekula, T. Mappes, T. Schimmel and H. Fuchs, *Nat. Nanotechnol.*, 2010, **5**, 275.
14 S. Sekula, J. Fuchs, S. Weg-Remers, P. Nagel, S. Schuppler, J. Fragala, N. Theilacker, M. Franzreb, C. Wingren, P. Ellmark, C. A. K. Borrebaeck, C. A. Mirkin, H. Fuchs and S. Lenhert, *Small*, 2008, **4**, 1785.
15 S. Lenhert, P. Sun, Y. Wang, H. Fuchs and C. A. Mirkin, *Small*, 2007, **3**, 71.
16 J. T. Groves and S. G. Boxer, *Acc. Chem. Res.*, 2002, **35**, 149.
17 C.-h. Yu and J. T. Groves, *Med. Biol. Eng. Comput.*, 2010, **48**, 955.
18 I. Czolkos, A. Jesorka and O. Orwar, *Soft Matter*, 2011, **7**, 4562.
19 E. Sackmann, *Science*, 1996, **271**, 43.
20 A. L. DeMond, K. D. Mossman, T. Starr, M. L. Dustin and J. T. Groves, *Biophys. J.*, 2008, **94**, 3286.
21 R. Sennett and G. Scott, *J. Opt. Soc. Am.*, 1950, **40**, 203.
22 B. D. Gates, Q. Xu, M. Stewart, D. Ryan, C. G. Willson and G. M. Whitesides, *Chem. Rev.*, 2005, **105**, 1171.
23 J.-M. Alakoskela, A. L. Koner, D. Rudnicka, K. Koehler, M. Howarth and D. M. Davis, *Biophys. J.*, 2011, **100**, 2865.
24 H. Krobath, B. Różycki, R. Lipowsky and T. R. Weikl, *PLoS One*, 2011, **6**, e23284.
25 T. Lohmüller, S. Triffo, G. P. O'Donoghue, Q. Xu, M. P. Coyle and J. T. Groves, *Nano Lett.*, 2011, **11**, 4912.
26 R. D. Piner, J. Zhu, F. Xu, S. Hong and C. A. Mirkin, *Science*, 1999, **283**, 661.
27 K. Salaita, Y. Wang and C. A. Mirkin, *Nat. Nanotechnol.*, 2007, **2**, 145.
28 W. Shim, A. B. Braunschweig, X. Liao, J. Chai, J. K. Lim, G. Zheng and C. A. Mirkin, *Nature*, 2011, **469**, 516.
29 F. Huo, Z. Zheng, G. Zheng, L. R. Giam, H. Zhang and C. A. Mirkin, *Science*, 2008, **321**, 1658.
30 K. Lee, S. Park, C. Mirkin, J. Smith and M. Mrksich, *Science*, 2002, **295**, 1702.
31 D. L. Wilson, R. Martin, S. Hong, M. Cronin-Golomb, C. A. Mirkin and D. L. Kaplan, *Proc. Natl. Acad. Sci. U. S. A.*, 2001, **98**, 13660.
32 R. McKendry, W. Huck, B. Weeks, M. Florini, C. Abell and T. Rayment, *Nano Lett.*, 2002, **2**, 713.
33 A. Hernandez-Santana, E. Irvine, K. Faulds and D. Graham, *Chem. Sci.*, 2011, **2**, 211.
34 J. Lim and C. A. Mirkin, *Adv. Mater.*, 2002, **14**, 1474.
35 M. Yu, D. Nyamjav and A. Ivanisevic, *J. Mater. Chem.*, 2005, **15**, 649.
36 B. L. Jackson and J. T. Groves, *J. Am. Chem. Soc.*, 2004, **126**, 13878.
37 V. Silin, H. Wieder, J. Woodward, G. Valincius, A. Offenhausser and A. Plant, *J. Am. Chem. Soc.*, 2002, **124**, 14676.
38 N. Kohli, S. Vaidya, R. Y. Ofoli, R. M. Worden and I. Lee, *J. Colloid Interface Sci.*, 2006, **301**, 461.
39 G. Luo, T. Liu, X. Zhao, Y. Huang, C. Huang and W. Cao, *Langmuir*, 2001, **17**, 4074.
40 L. Zhang, M. Longo and P. Stroeve, *Langmuir*, 2000, **16**, 5093.
41 C. Ma, M. Srinivasan, A. Waring, R. Lehrer, M. Longo and P. Stroeve, *Colloids Surf., B*, 2003, **28**, 319.
42 K. Salaita, Y. Wang, J. Fragala, R. A. Vega, C. Liu and C. A. Mirkin, *Angew. Chem., Int. Ed.*, 2006, **45**, 7220.
43 X. Liao, A. B. Braunschweig and C. A. Mirkin, *Nano Lett.*, 2010, **10**, 1335.
44 R. Garcia and R. Perez, *Surf. Sci. Rep.*, 2002, **47**, 197.
45 R. McAloney, M. Sinyor, V. Dudnik and M. Goh, *Langmuir*, 2001, **17**, 6655.
46 M. Dahlgren, P. Claesson and R. Audebert, *J. Colloid Interface Sci.*, 1994, **166**, 343.
47 S. Dubas and J. Schlenoff, *Macromolecules*, 1999, **32**, 8153.
48 M. N. Costa, K. Radhakrishnan and J. S. Edwards, *J. Biotechnol.*, 2011, **151**, 261.
49 E. G. Hofman, A. N. Bader, J. Voortman, D. J. van den Heuvel, S. Sigismund, A. J. Verkleij, H. C. Gerritsen and P. M. P. v. B. E. Henegouwen, *J. Biol. Chem.*, 2010, **285**, 39481.
50 I. Chung, R. Akita, R. Vandlen, D. Toomre, J. Schlessinger and I. Mellman, *Nature*, 2010, **464**, 783.
51 D. S. Lidke, K. A. Lidke, B. Rieger, T. M. Jovin and D. J. Arndt-Jovin, *J. Cell Biol.*, 2005, **170**, 619.
52 J.-M. Nam, P. M. Nair, R. M. Neve, J. W. Gray and J. T. Groves, *ChemBioChem*, 2006, **7**, 436.
53 O. Theodoly, Z. H. Huang and M. P. Valignat, *Langmuir*, 2010, **26**, 1940.
54 D. R. Stabley, C. Jurchenko, S. S. Marshall and K. S. Salaita, *Nat. Methods*, 2011, DOI: 10.1038/nmeth.1747.

Published on 01 December 2011 on http://pubs.rsc.org | doi:10.1039/C1SC00475A
Downloaded on 03 December 2011

 This journal is © The Royal Society of Chemistry 2011